

Properties of magnetic nanoparticles in the Brownian relaxation range for liquid phase immunoassays

K. Enpuku,^{a)} T. Tanaka, and T. Matsuda

Research Institute of Superconductor Science and Systems, Kyushu University, Fukuoka 819-0395, Japan

F. Dang, N. Enomoto, and J. Hojo

Department of Applied Chemistry, Kyushu University, Fukuoka 819-0395, Japan

K. Yoshinaga

Department of Applied Chemistry, Kyushu Institute of Technology, Kitakyushu 804-8550, Japan

F. Ludwig, F. Ghaffari, E. Heim, and M. Schilling

Institute of Electrical Measurement and Fundamental Electrical Engineering, TU Braunschweig, Hans-Sommer-Str. 60, D-38106 Braunschweig, Germany

(Received 15 April 2007; accepted 14 July 2007; published online 4 September 2007)

Properties of magnetic nanoparticles in the Brownian relaxation region were studied. Using the magnetic nanoparticles that exhibit remanence, we measured the magnetic properties, such as static magnetization, magnetic relaxation, and alternating current susceptibility, in a solution. Comprehensive comparisons were made between the experimental results and the theoretical ones predicted from the Brownian relaxation. From the comparison, the distributions of the particle parameters, i.e., the magnetic moment and the relaxation time, were estimated. It was shown that all the magnetic properties can be well explained when we take into account the parameter distributions in the sample. © 2007 American Institute of Physics. [DOI: [10.1063/1.2775882](https://doi.org/10.1063/1.2775882)]

I. INTRODUCTION

Immunoassays are widely used to detect disease-related proteins for medical diagnosis. These proteins are generically called antigens and the so-called binding reaction between antigen and its antibody is used for the immunoassay. Recently, magnetic immunoassays utilizing magnetic markers and magnetic sensors have been studied.^{1–15} In this method, an antibody is labeled with the magnetic marker made of magnetic nanoparticles and the binding reaction is detected by measuring the magnetic signal from the marker.

One of the merits of this magnetic method is that we can perform immunoassay in the liquid phase. This function can be realized by utilizing magnetic relaxation phenomena caused by Brownian rotation of the magnetic markers in a solution. Using the phenomena, we can distinguish bound markers from unbound (free) ones without using the so-called bound/free (BF) separation process. Since the time-consuming process of the BF separation can be eliminated, we can expect a high-speed immunoassay with the magnetic method.

Liquid phase immunoassays have so far been demonstrated using the magnetization curve,^{3,4} magnetic relaxation after the external field is turned off,^{5–10} and the frequency dependence of the alternating current (ac) susceptibility.^{11–13} Since the performance of the immunoassay is determined by the magnetic properties of the marker in a solution, it is important to clarify these properties for the improvement of the liquid phase immunoassay. However, they have not yet been fully clarified since they strongly depend on various particle parameters, such as particle size, distribution of par-

ticle size, and the degree of aggregation of the particles. Although these magnetic properties were measured independently, comprehensive comparison among these properties has not yet been made.

In this article, we study the properties of magnetic nanoparticles in a solution. We use particles that keep remanence, instead of the so-called superparamagnetic ones, since we have been developing the immunoassay using these particles.^{10,14,15} The magnetic properties are determined by measuring the magnetization curve, the magnetic relaxation, and the ac susceptibility. Comprehensive comparisons are made between the experimental results and the theoretical ones predicted from the Brownian relaxation. From the comparison, the distributions of the particle parameters, such as magnetic moment, relaxation time, and particle size, are estimated. The estimated distribution of the particle size is also compared to that obtained from dynamic light scattering (DLS) measurements.

II. MAGNETIC PROPERTIES IN LIQUID

A. Sample

The silica-coated Fe₃O₄ nanoparticles were fabricated as follows. The Fe₃O₄ particles were synthesized via oxidation of Fe(OH)₂ in alkaline solution. Then tetraethylorthosilicate diluted with ethanol was added to the alkaline suspension to fabricate the silica coating. All of the processes were executed under ultrasonication¹⁶ to enhance the oxidation and hydrolysis, and also to minimize agglomeration.

The Fe₃O₄ particles were designed so that they are not superparamagnetic but exhibit remanence. From transmis-

^{a)}Electronic mail: enpuku@sc.kyushu-u.ac.jp

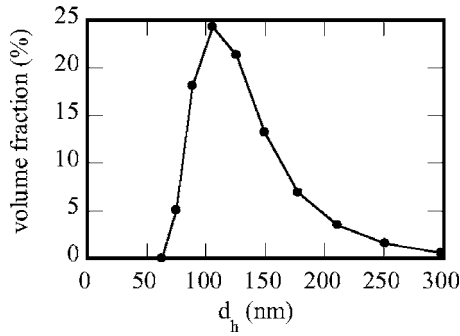


FIG. 1. Distribution of the hydrodynamic diameter of the silica coated Fe_3O_4 particles measured with DLS. The vertical axis represents the volume fraction of the particles.

sion electron microscopy (TEM) measurements, the shape of Fe_3O_4 particle was determined to be cubic-like, and the size amounts to typically 30 nm.

The hydrodynamic diameter of the particle was measured utilizing DLS. The result is shown in Fig. 1 where the vertical axis represents the volume fraction of the particles. The mean diameter of the particles amounts to 105 nm. This value is considerably larger than the value of 30 nm measured with TEM. Therefore, aggregation occurred in the fabrication process.

The magnetization curve of the dried sample was measured with a vibrating sample magnetometer (VSM). In Fig. 2, the M - H curve measured on a powder sample of the Fe_3O_4 particles is depicted. From the curve, we estimated a saturation magnetization $\mu_0 M_s = 340$ mT and a remanence $\mu_0 M_r = 80$ mT. The apparent coercive field that produced $M=0$ was 10 mT.

B. M - H curve

In Fig. 3, the M - H curve of the sample in a solution is shown, which was measured with a homemade magnetometer using a magnetoresistance sensor. The vertical axis represents the magnetization normalized by the saturation value M_{sat} at $\mu_0 H = 2$ mT. As shown, the value of M increased and then began to saturate with the increase of the external field H . Although this behavior is similar to that of the superparamagnetic particle, we note that the saturation of M occurred at very low values of H in the present case, i.e., at about $\mu_0 H = 1.5$ mT. In the case of superparamagnetic particles,

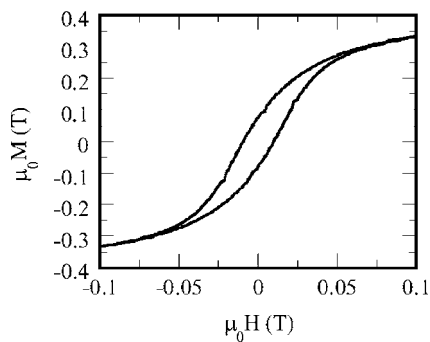


FIG. 2. Magnetization curve of the dried sample measured with VSM. Powder of the Fe_3O_4 particles was used as sample.

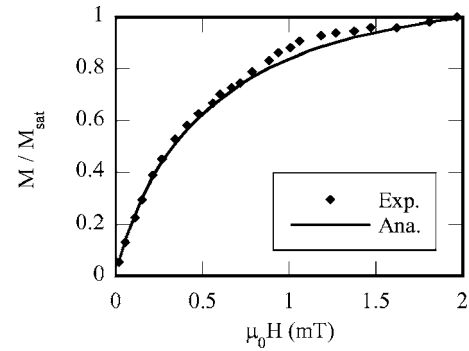


FIG. 3. M - H curve of the silica coated Fe_3O_4 particles in a solution. Symbols are experimental results, while the solid line is calculated from Eq. (1) with the parameters listed in Table I.

saturation of M occurs between 100 mT and 1 T.^{11,12} This difference will be due to the existence of the remanence M_r in the present particle.

It is known that the M - H curve of the magnetic nanoparticles in a solution is subjected by the Brownian rotation. When we take into account the distribution of the particle size in the sample, the M - H curve is given by

$$M(H) = \frac{1}{V} \sum_i n_i m_i L[\alpha_i(H)] = M_{\text{sat}} \sum_i w_i L[\alpha_i(H)] \quad (1)$$

with

$$L(x) = \coth(x) - 1/x, \quad (2)$$

where V is the volume of the sample, $L(x)$ is the Langevin function, which depends on the dimensionless Langevin parameter $\alpha_i(H) = m_i H / kT$, k is the Boltzmann's constant, T is the absolute temperature, and w_i are the so-called magnetic weights. The magnetic weight is defined by $w_i = n_i m_i / \sum_i n_i m_i$, where n_i is the number of particles with magnetic moment m_i . We use here the magnetic weight w_i for the distribution since w_i is proportional to the volume fraction of particles with magnetic moment m_i and diameter d_{mi} , respectively, and which thus can be compared to the results from DLS measurements. The magnetic moment m_i is given by $m_i = \mu_0 M_{\text{sat}} (\pi/6) d_{mi}^3$, and M_{sat} is given by $M_{\text{sat}} = (1/V) \sum_i n_i m_i$, whose absolute value will be discussed in Sec. III.

The solid line in Fig. 3 is calculated from Eq. (1) with the values of m_i and w_i listed in Table I. The estimation procedure of the m_i and w_i values will be discussed in the next section. As shown, good agreement is obtained between experiment and the theoretical prediction.

C. Magnetic relaxation

We measured the relaxation of the sample magnetization M after the external field H was turned off from $H=H_0$. In the experiment, the external field of $\mu_0 H_0 = 2$ mT was applied for 2 s. At this field value, we can expect that all the magnetic moments of the particles are aligned since the magnetization M saturates at this field as shown in Fig. 3. Then, the external field was linearly turned off with a falling time of $T_0 = 0.15$ ms. The relaxation of $M(t)$ after the external field becomes $H=0$ was measured using a differential flux-

TABLE I. Estimated parameters of the sample. The values of τ_i and $w_i L_i$ are estimated with the nonlinear least-square method, while the values in brackets are estimated from the successive reduction method. Note that the successive reduction method data were taken as initial values for the nonlinear least-square method fit.

i	τ_i (ms)	$w_i L_i$ (%)	m_i/kT (10^{-3} m/A)	w_i (%)	$L(\alpha i)$ $\mu_0 H = 2$ mT
1	0.26 (0.31)	60.0 (59.5)	3.12	64.2	0.80
2	1.03 (1.05)	33.7 (33.5)	12.36	30.3	0.95
3	6.07 (5.74)	6.3 (7.0)	72.84	5.5	0.99

gate setup. Details of the measurement system are described elsewhere.^{17,18} In Fig. 4, the experimental decay of M with time is shown.

The relaxation of M due to the Brownian rotation is given by

$$M(t)/M_{\text{sat}} = \sum_i M_i(t) = \sum_i w_i L_i [\alpha_i(H_0)] \exp(-t/\tau_i) \text{ for } t > 0, \quad (3)$$

where τ_i is the relaxation time given by

$$\tau_i = 3\eta(\pi/6)d_{hi}^3/kT, \quad (4)$$

where η is the viscosity of the carrier liquid and d_{hi} is the hydrodynamic diameter of the particle. We note that the effect of finite switch-off time T_0 is neglected in Eq. (3). This assumption is valid when the relaxation times τ_i are larger than the falling time T_0 .

As shown in Fig. 4, the value of $\ln M$ does not decrease linearly with time. This means the existence of several relaxation times. To estimate typical values of τ_i , which can be used as initial values for more accurate estimation procedures, we first applied the so-called successive reduction technique. The estimation procedure is shown in Fig. 5. First, the longest relaxation time τ_1 and the amplitude $w_1 L_1$ are estimated by using the experimental data at longer times. In this time range, we assume $M(t) = M_1(t) = w_1 L_1 \exp(-t/\tau_1)$ by neglecting the components with shorter relaxation times.

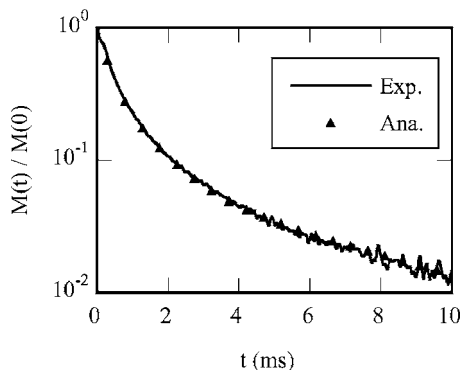


FIG. 4. Magnetic relaxation $M(t)$ after the external field is turned off from $\mu_0 H_0 = 2$ mT. The solid line is the experimental result, while the symbols are calculated from Eq. (3) with the parameters listed in Table I.

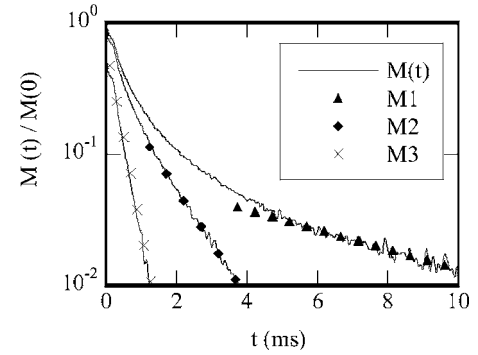


FIG. 5. Procedure of successive reduction for the estimation of time constants.

Then, the values of τ_2 and $w_2 L_2$ are estimated by assuming $M(t) - M_1(t) = M_2(t) = w_2 L_2 \exp(-t/\tau_2)$. This process is performed successively.

For the present sample, we obtained three values of τ_i and $w_i L_i$, which are given by the values in brackets in Table I. We note, however, that the mathematical accuracy of the successive reduction technique is not so clear due to the arbitrariness in the definition of the intervals of the successive steps. Therefore, we applied the so-called nonlinear least-square method in order to make a more accurate estimation of the parameters τ_i and $w_i L_i$. In this method, the norm σ^2 determined by

$$\sigma^2 = \sum_j [M_{\text{exp}}(t_j) - M_{\text{ana}}(t_j)]^2 \quad (5)$$

is minimized with respect to the parameters τ_i and $w_i L_i$, where the $M_{\text{exp}}(t_j)$ values are the experimental data, and the $M_{\text{ana}}(t_j)$ are the corresponding values calculated with Eq. (3). Since M_{ana} nonlinearly depends on the parameter τ_i , the minimization of the norm σ^2 is done with the nonlinear least-square method. For this purpose, we used the commercial program installed in MATLAB (The Mathworks, Inc., Natick, MA, USA). In applying the method, the initial values of the parameters affect the accuracy of the estimation to a large extent. In the present case, we used the values obtained with the successive reduction technique as initial values.

The estimated values of τ_i and $w_i L_i$ are listed in Table I. We note that the parameters estimated with the nonlinear least-square method are nearly the same as those estimated with the successive reduction technique. The symbols in Fig. 4 represent the $M(t)$ curve calculated from Eq. (3) with these parameters. As shown, the calculated result agrees well with the experimental one. The accuracy of the parameter estimation is evaluated by the norm given in Eq. (5). The normalized uncertainty of $\sigma/\sum M_{\text{exp}}(t_j) = 2.6 \times 10^{-3}$ was reasonably small.

In order to prove consistency between the M - H and the relaxation data, we estimated the values m_i from the value of τ_i . Using Eq. (4) and the expression for m_i , the relationship between m_i and τ_i is given by $m_i/kT = (\mu_0 M_{\text{sat}}/3\eta)(d_{mi}^3/d_{hi}^3)\tau_i$. Since, however, the exact value of M_{sat} and the relation between d_{mi} and d_{hi} are not known, we tentatively introduce an adjustable parameter $A = (\mu_0 M_{\text{sat}}/3\eta)(d_{mi}^3/d_{hi}^3)$, and assume a linear relation $m_i/kT = A\tau_i$. Using the relation, we

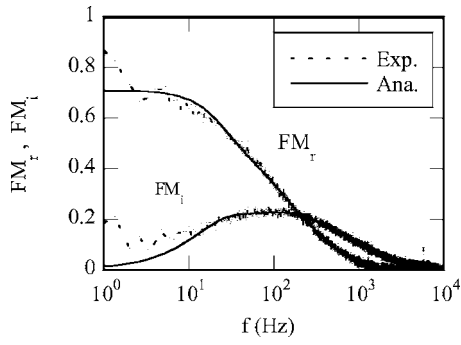


FIG. 6. Fourier transform of the relaxation curve $M(t)$ shown in Fig. 4. FM_r and FM_i are the real and the imaginary part, respectively. The broken lines are experimental data, while the solid lines are calculated from Eq. (6) with the parameters listed in Table I.

can estimate m_i from τ_i . The value of A was chosen so as to obtain the best fit between the experimental M - H curve and Eq. (1). A value of $A=12$ gives the best fit as shown in Fig. 3, and the corresponding magnetic moments m_i are listed in Table I. A discussion of the value of A is performed in Sec. III. The magnetic weights w_i are also calculated from the values of $w_i L(\alpha_i)$ using the value of $L(\alpha_i)$ at $\mu_0 H=2$ mT.

For the following discussion, we make a Fourier transform of the relaxation curve $M(t)$. In Fig. 6, the Fourier transform of the experimental $M(t)$ curve is shown. Here, FM_r and FM_i are the real and the imaginary part, respectively. As shown, the real part is flat in the low frequency region, and decreases with the frequency. The imaginary part has a broad peak around the frequency $f=100$ Hz.

The Fourier transform of Eq. (3) is given by

$$FM(f) = FM_r(f) + jFM_i(f) = \sum_i w_i L[\alpha_i(H_0)] \frac{\tau_i}{1 + j2\pi f \tau_i}. \quad (6)$$

The solid lines in Fig. 6 are calculated from Eq. (6) with the parameters listed in Table I. As shown, good agreement is obtained between experiment and Eq. (6).

D. ac susceptibility

We studied the frequency dependence of the ac susceptibility. In the experiment, an ac field with an amplitude of $\mu_0 H=0.28$ mT was applied in order to use the linear region of the M - H curve as shown in Fig. 3. The frequency dependence of the susceptibility χ is shown in Fig. 7. Here, χ_r and χ_i are the real and imaginary part of the susceptibility, respectively. As shown the real part decreases with frequency, while the imaginary part has a broad peak around $f=250$ Hz.

For the case of a small external field H , i.e., when $L(H)$ is proportional to H , the frequency dependence of the susceptibility due to the Brownian rotation is given by

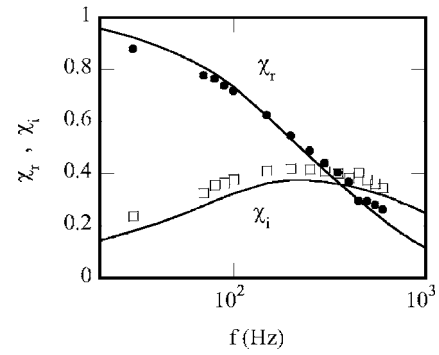


FIG. 7. Frequency dependence of the real part χ_r and the imaginary part χ_i of the ac susceptibility. The symbols are experimental data, while the solid lines are calculated from Eq. (7) with the parameters listed in Table I.

$$\begin{aligned} \chi(f) = \chi_r(f) + j\chi_i(f) &= \sum_i \frac{w_i L[\alpha_i(H)]}{H} \frac{1}{1 + j2\pi f \tau_i} \\ &= \sum_i \frac{w_i m_i}{3kT} \frac{1}{1 + j2\pi f \tau_i}, \end{aligned} \quad (7)$$

where χ is the ac susceptibility normalized by the direct current susceptibility.

In Fig. 7, the solid lines are calculated from Eq. (7) with the parameters listed in Table I. Again, good agreement is obtained between experiment and Eq. (7).

We note that Eqs. (6) and (7) give the same frequency dependence when the sample has a single relaxation time. This means that the Fourier transform of the relaxation and the frequency dependence of the susceptibility are equivalent to each other.¹⁹ However, the frequency dependence of Eqs. (6) and (7) becomes different when many relaxation times exist in the sample. Thus, for example, the frequencies at which the peak of the imaginary part occurs are different in the two cases. As can be seen from Figs. 6 and 7, the peak appears at $f=100$ Hz for FM_i and at $f=250$ Hz for χ_i .

III. DISTRIBUTION OF PARTICLE PARAMETERS

As shown earlier, all the magnetic properties in liquid can be explained well with the particle parameters listed in Table I. However, only a small number of relaxation times can be estimated with the nonlinear least-square method. On the other hand, several methods have been developed to estimate the distribution of the particle size from the M - H curve.^{20,21} In the following, we use the so-called singular value decomposition (SVD) method to estimate the distribution of the magnetic moment m_i of the particle.

Details of the SVD method were described in Ref. 20. Briefly, we assume N sets m_i in Eq. (1) with unknown values of w_i . We use K sets of M_j and H_j obtained from the experimental results shown in Fig. 3, where $K > N$. Then, we obtain the equation

$$M_j = \sum_{i=1}^N w_i L(m_i H_j / kT) \quad \text{for } j = 1, \dots, K. \quad (8)$$

Introducing the vector \mathbf{M} and \mathbf{w} with components M_j and w_i , and the $K \times N$ matrix \mathbf{A} with components $A_{ji} = L(m_i H_j / kT)$, we can express Eq. (8) as $\mathbf{M} = \mathbf{A}\mathbf{w}$. Then, the matrix is de-

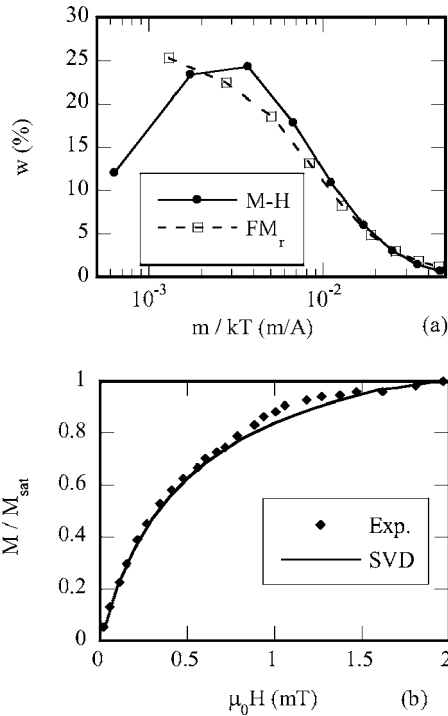


FIG. 8. (a) Distribution of the magnetic weight w_i as a function of magnetic moment m_i/kT . Closed symbols are estimated from the M - H curve shown in Fig. 3. Open symbols represent the distribution converted from the τ_i - $w_i L_i$ curve shown in Fig. 9(a), which was obtained from FM_r data. (b) Comparison of the experimental M - H curve with that reconstructed from the m_i - w_i distribution given by the closed symbols in (a).

composed as $\mathbf{A}=\mathbf{U}\mathbf{S}\mathbf{V}^T$, where \mathbf{U} and \mathbf{V} are correspondingly $K \times K$ and $N \times N$ orthogonal matrices and \mathbf{S} is the $K \times N$ diagonal matrix with the nonzero elements s_{ii} , which are called singular values of \mathbf{A} . Using the matrices \mathbf{U} , \mathbf{S} , and \mathbf{V} , we can calculate $\mathbf{V}^T \mathbf{w} = \mathbf{S}^T \mathbf{U}^T \mathbf{M}$. In the SVD method, we introduce some threshold value s_{min} . For the value of $s_{ii} > s_{min}$, components of the matrix $\mathbf{S}^T \mathbf{U}^T \mathbf{M}$ are calculated, while the components are set to zero for $s_{ii} < s_{min}$. In other words, we take n singular values which satisfy $s_{ii} > s_{min}$. Then, we can estimate the vector $\mathbf{w} = \mathbf{V}\mathbf{S}^T \mathbf{U}^T \mathbf{M}$. The threshold value s_{min} (or the number n) is determined so as to obtain the best fit between the experimental M - H curve and the analytical curve reconstructed with the vector \mathbf{w} .

Using the earlier procedure, we can estimate the weight distribution w_i as a function of the magnetic moment m_i . In Fig. 8(a), closed symbols show the w_i distribution estimated from the M - H curve shown in Fig. 3. In the estimation procedure, we take the three largest values of the singular values. As depicted in Fig. 8(a), we obtained the w_i distribution in the range of $6 \times 10^{-4} < m_i/kT < 1 \times 10^{-1}$. The accuracy of the parameter estimation is evaluated by the norm σ^2 given in Eq. (5). In the present case, the normalized uncertainty of $\sigma/\sum M_{exp}(H_j) = 4.6 \times 10^{-3}$ was again sufficiently small.

We note that the M - H curve reconstructed from the m_i - w_i distribution determined with the SVD method agrees well with the experimental one, as shown in Fig. 8(b). Comparing the M - H curves calculated with the SVD [cf. Fig. 8(b)] and with the nonlinear least-square method (cf. Fig. 3) no differences are discernable.

Using the same procedure, we can estimate the param-

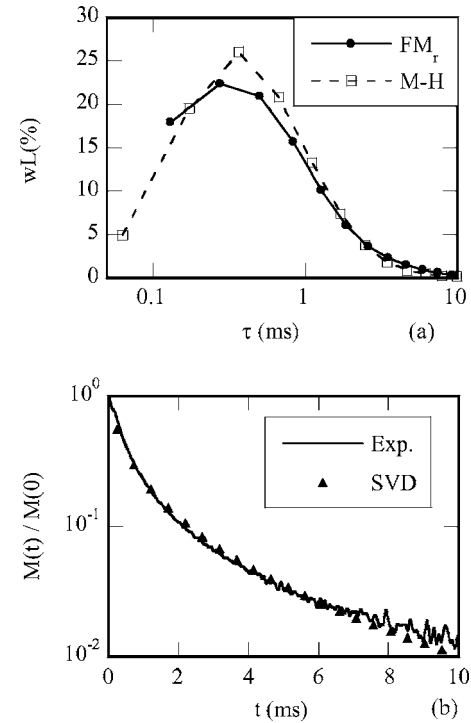


FIG. 9. (a) Distribution of the magnetic weight $w_i L_i$ as a function of relaxation time τ_i . Closed symbols are estimated from the FM_r curve shown in Fig. 6. Open symbols represent the distribution converted from the m_i - w_i curve shown in Fig. 8(a), which was obtained from the M - H data. (b) Comparison of the experimental $M(t)$ curve with that reconstructed from the τ_i - $w_i L_i$ distribution given by the closed symbols in (a).

eter distribution from the magnetic relaxation $M(t)$ shown in Fig. 4. In this case, we can estimate the distribution $w_i L_i(\alpha_i)$ as a function of the time constant τ_i . We note, however, that more reliable results are obtained when the real part of the Fourier transform FM_r is used. Therefore, the estimation was performed using the FM_r data shown in Fig. 6 and Eq. (6). In Fig. 9(a), closed symbols show the estimated $w_i L_i$ distribution versus time constant τ_i . As can be seen, we obtained the $w_i L_i$ distribution in the range of $0.13 \text{ ms} < \tau_i < 10 \text{ ms}$. We note that the $M(t)$ curve reconstructed from the τ_i - $w_i L_i$ distribution agrees well with the experimental one, as shown in Fig. 9(b). The accuracy of the parameter estimation is evaluated by the normalized uncertainty as $\sigma/\sum M_{exp}(t_j) = 5.9 \times 10^{-3}$. As for the analysis of the M - H curves, no differences are discernable between the $M(t)$ curves calculated with the SVD [cf. Fig. 9(b)] and with the nonlinear least-square method (cf. Fig. 4).

We now discuss the relation between the parameter distributions shown in Figs. 8(a) and 9(a). Since the thickness of the silica coating is very thin in the present case, we tentatively assume $d_{hi} = d_{mi}$. In this case, the linear relationship between m_i and τ_i simplifies to $m_i/kT = (\mu_0 M_{sat}/3\eta)\tau_i = A\tau_i$. Using this relation and Eq. (2), we can relate the w_i - m_i and $w_i L_i$ - τ_i curves to each other. In Fig. 8(a), open symbols represent the w_i - m_i curve converted from the $w_i L_i$ - τ_i curve with the parameter $A=10$. Similarly, open symbols in Fig. 9(a) represent the $w_i L_i$ - τ_i curve converted from the w_i - m_i curve with the same parameter $A=10$. As shown, reasonable agreement is obtained in both cases. This agreement shows

the consistency between the M - H and the relaxation data. Note that a value $A=12$ was also obtained relating the nonlinear least-square method analysis of the M - H and relaxation data. The consistency of the value of A between the SVD and the nonlinear least-square method indicates the reliability of the obtained results.

Although it is enough to know the w_i - m_i and $w_i L_i$ - τ_i curves for the magnetic properties in liquid, we can also estimate other particle parameters that determine m_i and τ_i . First, we discuss the saturation value of M_{sat} . Using the relation of $A=(\mu_0 M_{\text{sat}}/3\eta)(d_{\text{mi}}^3/d_{\text{hi}}^3)$, we obtained $\mu_0 M_{\text{sat}}=30$ mT from the values of $A=10$ and $\eta=1.0 \times 10^{-3}$ Pa s for water and assuming $d_{\text{mi}}=d_{\text{hi}}$.

We note that the absolute value of M_{sat} can, in principle, be obtained from the M - H curve shown in Fig. 3 if we know the coupling parameter K that combines the magnetization M of the sample and the magnetic field B measured with the magnetic sensor, i.e., $M=B/K$. Since, however, the parameter K complicatedly depends on the geometry of the measurement system, it is difficult to obtain an exact value of K of the present system. We evaluated the value of K with a rough calibration of our measurement system and obtained that the saturation value M_{sat} was between $\mu_0 M_{\text{sat}}=20$ mT and $\mu_0 M_{\text{sat}}=50$ mT. The estimated value of $\mu_0 M_{\text{sat}}=30$ mT is within this region.

We note that the estimated value of $\mu_0 M_{\text{sat}}=30$ mT is much smaller than the values of $\mu_0 M_s=340$ mT and $\mu_0 M_r=80$ mT shown in Fig. 2, which were measured on a dried sample by applying a high external field. One possible reason for this discrepancy could be the aggregation of particles. When aggregation of particles occurs, the magnetic moments of the individual particles within an agglomerate are not aligned in the same direction, i.e., an aggregated particle will behave like a multidomain particle rather than a single-domain one. As a result, the saturation magnetization of an aggregated particle in liquid will be smaller than that of a single-domain one. The quantitative discussion of M_{sat} of the present particles, which exhibit remanence, aggregation and saturation in weak external fields, is a problem that remains to be solved.

Next, we estimate the distribution of the hydrodynamic diameter d_{hi} of the particles from the $w_i L_i$ - τ_i curves shown in Fig. 9(a) and compare the results with the DLS measurement shown in Fig. 1. In Fig. 10, the w_i - d_{hi} curves converted from the $w_i L_i$ - τ_i curves are shown. Here, d_{hi} was estimated from τ_i using the relation $\tau_i=3\eta(\pi/6)d_{\text{hi}}^3/kT$ with $\eta=1 \times 10^{-3}$ Pa s for water. We note that the magnetic weight w_i is equal to the volume fraction of the particles measured with DLS. As shown in Fig. 10, reasonable agreement is obtained between the distribution determined from DLS measurements and those estimated from the magnetic properties, though the value of d_{hi} estimated from the magnetic measurements is—especially for small d_{hi} values—slightly smaller than that from the DLS experiment. We note that the DLS measurement is obtained from the Brownian motion of the particles, while the magnetic properties are determined by the Brownian rotation. Therefore, the earlier result indicates that the hydrodynamic diameters estimated from the Brownian motion and the Brownian rotation reasonably agree with each

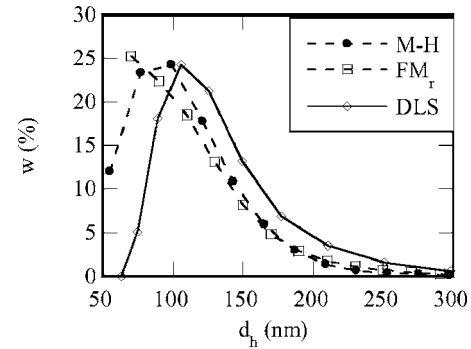


FIG. 10. Distribution of the volume fraction as a function of the hydrodynamic diameter d_h of the particles. Distributions estimated from the M - H and FM_r curves are compared with that obtained from the optical DLS measurement.

other. The observed discrepancies might be due to deviations from a spherical particle shape which is assumed for the analysis of DLS as well as of magnetic measurements.

IV. CONCLUSION

We studied the properties of magnetic nanoparticles in the Brownian relaxation regime. Using magnetic nanoparticles that keep remanence, we measured the magnetic properties, such as static magnetization, magnetic relaxation, and ac susceptibility, in a solution. It was shown that all the magnetic properties can be well explained with the theoretical ones predicted from the Brownian relaxation when we take into account the particle parameter distributions in the sample. From the comparison, the distributions of particle parameters, such as magnetic moment, relaxation time, and particle size, are estimated. The estimated distribution of the particle size reasonably agrees with that obtained from DLS measurements.

ACKNOWLEDGMENTS

Financial support by the Japanese Grant-in Aid for Scientific Research (B) and the Deutsche Forschungsgemeinschaft via Grant No. SFB 578 is acknowledged.

- ¹R. Kötitz, H. Matz, L. Trahms, H. Koch, W. Weitschies, T. Rheinländer, W. Semmler, and T. Bunte, IEEE Trans. Appl. Supercond. **7**, 3678 (1997).
- ²K. Enpuku, T. Minotani, T. Gima, Y. Kuroki, Y. Itoh, M. Yamashita, Y. Katakura, and S. Kuhara, Jpn. J. Appl. Phys., Part 2 **38**, L1102 (1999).
- ³K. Kriz, J. Gehrke, and D. Kriz, Biosens. Bioelectron. **13**, 817 (1998).
- ⁴C. Y. Hong, C. C. Wu, Y. C. Chiu, S. Y. Yang, H. E. Horng, and H. C. Yang, Appl. Phys. Lett. **88**, 212512 (2006).
- ⁵J. Lange, R. Kötitz, A. Haller, L. Trahms, W. Semmler, and W. Weitschies, J. Magn. Magn. Mater. **252**, 381 (2002).
- ⁶H. Grossman, W. Myers, V. Vreeland, R. Bruehl, M. Alper, C. Bertozzi, and J. Clarke, Proc. Natl. Acad. Sci. U.S.A. **101**, 129 (2004).
- ⁷D. Eberbeck, C. Bergemann, S. Hartwig, U. Steinhoff, and L. Trams, J. Magn. Magn. Mater. **289**, 435 (2005).
- ⁸G. Glöckl, V. Brinkmeier, K. Aurich, E. Romanus, P. Weber, and W. Weitschies, J. Magn. Magn. Mater. **289**, 480 (2005).
- ⁹H. C. Yang, S. Y. Yang, G. L. Fang, W. H. Huang, C. H. Liu, S. H. Liao, H. E. Horng, and C. Y. Hong, J. Appl. Phys. **99**, 124701 (2006).
- ¹⁰K. Enpuku, K. Soejima, T. Nishimoto, H. Tokumitsu, H. Kuma, N. Hamasaki, and K. Yoshinaga, J. Appl. Phys. **100**, 054701 (2006).
- ¹¹A. P. Astalan, F. Ahrentorp, C. Johansson, K. Larsson, and A. Krozer, Biosens. Bioelectron. **19**, 945 (2004).
- ¹²S. H. Chung, A. Hoffmann, K. Guslienko, S. D. Bader, C. Liu, B. Kay, L.

- Makowski and L. Chen, J. Appl. Phys. **97**, 10R101 (2005).
- ¹³Y. Bao, A. B. Pakhomov, and K. M. Krishnan, J. Appl. Phys. **99**, 08H107 (2006).
- ¹⁴K. Enpuku, D. Kuroda, T. Q. Yang, and K. Yoshinaga, IEEE Trans. Appl. Supercond. **13**, 371 (2003).
- ¹⁵K. Enpuku, K. Inoue, K. Soejima, K. Yoshinaga, H. Kuma, and N. Hamasaki, IEEE Trans. Appl. Supercond. **15**, 660 (2005).
- ¹⁶N. Enomoto, J. Akagi, and Z. Nakagawa, Ultrason. Sonochem. **3**, S97 (1996).
- ¹⁷F. Ludwig, E. Heim, S. Mäuselein, D. Eberbeck, and M. Schilling, J. Magn. Magn. Mater. **293**, 690 (2005).
- ¹⁸F. Ludwig, S. Mäuselein, E. Heim, and M. Schilling, Rev. Sci. Instrum. **76**, 106102 (2005).
- ¹⁹P. C. Fannin, Adv. Chem. Phys. **104**, 181 (1998).
- ²⁰D. V. Berkov, P. Görnert, N. Buske, C. Gansau, J. Müller, M. Giersig, W. Neumann, and D. Su, J. Phys. D **33**, 331 (2000).
- ²¹J. P. Embs, S. May, C. Wagner, A. V. Kityk, A. Leschhorn, and M. Lücke, Phys. Rev. E **73**, 036302 (2006).